Two-dimensional (2+*n*) resonance enhanced multiphoton ionization of HCl: Photorupture channels via the $F\,^1\Delta_2$ Rydberg state and *ab initio* spectra

Ágúst Kvaran,[a] Huasheng Wang, Kristján Matthiasson, Andras Bodi, and Erlendur Jónsson
Science Institute, University of Iceland, Dunhagi 3, 107 Reykjavík, Iceland

(Received 17 June 2008; accepted 15 September 2008; published online 27 October 2008)

Mass spectra were recorded for (2+*n*) resonance enhanced multiphoton ionization (REMPI) of HCl as a function of resonance excitation energy in the 82 600–88 100 cm^{-1} region to obtain two-dimensional REMPI data. Analysis of ion-mass signal intensities for excitations via the $F\,^1\Delta_2(v'=0-2)$ and the $V\,^1\Sigma^+(v')$ states as a function of rotational quantum numbers in the intermediate states either revealed near-resonance interactions or no significant coupling between the $F\,^1\Delta_2$ and the $V\,^1\Sigma^+$ states, depending on quantum levels. Ion-signal intensities and power dependence measurements allowed us to propose photoionization mechanisms in terms of intermediate state involvement. Based on relative ion-signal intensities and rotational line positions we quantified the contributions of Rydberg and valence intermediate states to the photoionization product formation and evaluated coupling strengths for state mixing. Time-dependent density functional theory (TD-DFT), equation-of-motion coupled cluster (EOM-CC), and completely renormalized EOM-CC calculations with various basis sets were performed to derive singlet state potential energy curves, relevant spectroscopic parameters, and to calculate spectra. Experimentally observed spectra and older calculations are compared with the reported *ab initio* results. © *2008 American Institute of Physics*. [DOI: 10.1063/1.2996294]

INTRODUCTION

Hydrogen chloride is one of the most studied molecules in the fields of spectroscopy[1–17] and photoruptures (i.e., photodissociation and photoionization)[18–23] for a number of reasons. Quantitative data on molecule-photon interactions are of interest in understanding stratospheric photochemistry as well as being relevant to the photochemistry of planetary atmospheres and the interstellar medium.[4] Furthermore, relatively intense single- and multiphoton absorption in conjunction with electron excitations as well as rich band structured spectra make the molecule ideal for fundamental studies in these fields. Last but not least, detailed studies of resonance enhanced multiphoton ionization (REMPI) spectra of small molecules such as HCl are of importance in order to determine relative populations of quantum states in conjunction with frequent use of REMPI detection of product molecules in reaction dynamics.[11,24]

Since the original work by Price in 1938 on the hydrogen halides,[25] a wealth of spectroscopic data on HCl has been derived from high resolution absorption spectroscopy,[1–4] fluorescence studies,[4] and from REMPI experiments.[5–17] A large number of Rydberg states have been identified, as well as the $V(^1\Sigma^+)$ ion pair state. A number of spin-forbidden transitions are observed, indicating that spin-orbit coupling is important in excited states of the molecule. Perturbations due to state mixing are widely seen both in absorption[2–4] and REMPI spectra.[6,7,9,11,13,14,17] The perturbations appear either as line shifts[3,6,7,9,13,14,17] or as intensity and/or bandwidth alterations.[3,6,7,9,11,13,14,17] Pronounced ion pair to Rydberg state mixings are both observed experimentally[2,3,7,9,13,14,17,26] and predicted from theory.[26,27] Interactions between the $V(^1\Sigma^+)$ ion-pair state and the $E(^1\Sigma^+)$ state are found to be particularly strong and to exhibit nontrivial rotational, vibrational, and electron spectroscopies. Perturbations due to Rydberg-Rydberg mixings have also been predicted and identified.[3,11] Whereas most observed perturbation effects are believed to be homogeneous in nature ($\Delta\Omega=0$),[13,14,26,27] heterogeneous ($\Delta\Omega>0$) couplings have also been reported.[14,17,26]

Despite numerous experimental studies on the photochemistry and photophysics of the electronically excited states of HCl, only a limited number of theoretical studies have been performed on the excited states. The first *ab initio* calculations reported on the excited states of HCl, by Hirst and Guest only dealt with the valence states, emphasising vertical electronic transitions.[28] The pioneering work by Bettendorff *et al.*,[27] based on configuration interaction calculations and on the use of large atomic orbital basis sets, has served well for identifying and assigning electronically excited states, but is less useful for detailed quantitative comparison. More recently, Pradhan *et al.* have performed *ab initio* calculations on the ground and excited states of the HCl^+ ion.[29] Since the state-of-the-art work of Bettendorff *et al.* in 1982, a number of standard methods have been developed to handle excited states of molecules. Equation-

[a]Author to whom correspondence should be addressed. Tels.: +354-525-4694 and +354-525-4800. FAX: +354-552-8911. Electronic mail: agust@hi.is. URL: http://www.hi.is/~agust/.

of-motion coupled cluster (EOM-CC) theory[30] has been shown to reproduce experimental excitation energies very well in certain cases.[31] Recently, Pitarch-Ruiz *et al.* published calculations on vertical excitation energies to various Rydberg states of hydrogen chloride using a coupled-cluster approach.[32] We feel that it would also be of interest to apply such methods to study the potential energy curves relevant to electronic excitations and photorupture processes in HCl.

Photorupture studies of HCl have revealed a large variety of photodissociation and photoionization processes. Thus, photodissociation processes yielding excited states of both hydrogen and chlorine atoms have been observed.[33,34] Competition between autoionization and predissociation processes via a superexcited state has been identified and analyzed.[34] Superexcited states have been found to dissociate into electronically excited atomic fragments as well as to the $H^+ + X^-$ ion pair.[18] In a detailed two-photon REMPI study, Green *et al.* reported HCl^+, Cl^+, and H^+ ion formations for excitations via large number of $\Omega=0$ Rydberg states as well as via the $V\,^1\Sigma^+$ ($\Omega=0$) ion-pair state, whereas excitations via other Rydberg states are mostly found to yield HCl^+ ions.[6] More detailed investigations of excitations via various Rydberg states and the $V\,^1\Sigma^+$ ion-pair state by use of photofragment imaging and mass-resolved REMPI techniques have revealed several ionization channels depending on the nature of the resonance excited state.[19–22] Results are mostly based on analysis of excitations via the $E\,^1\Sigma^+$ Rydberg state and the $V\,^1\Sigma^+$ ion-pair state, which couple strongly to produce the mixed (adiabatic) $B\,^1\Sigma^+$ state with two minima, but to a lesser extent on analysis of excitations via triplet states, which show no coupling with the ion-pair state. These studies reveal characteristic ionization channels which can be summarized with reference to Fig. 1 as follows. For clarity we will distinguish between (1) resonance noncoupled (diabatic) Rydberg state excitations and (2) resonance noncoupled (diabatic) ion-pair excitations [see Fig. 1(b)]. The former could correspond to transitions via triplet Rydberg states which have not been found to couple to the ion-pair state, whereas the latter is an imaginary case of a "noncoupling" $V\,^1\Sigma^+$ state. Notice that in the case of a transition to a Rydberg state which couples to the $V\,^1\Sigma^+$ state, as well as to the $V\,^1\Sigma^+$ state itself (which does mix with a number of Rydberg states), both groups of excitation channels (1 and 2) will be involved. This is because it involves excitations to the adiabatic states which are obtained by a combination of the diabatic (noncoupling) states. Therefore those excitations will show characteristics according to the mixing of the diabatic components.

(1) An ionization via a noncoupled (diabatic) Rydberg state is found to involve (i) one-photon ionization of the Rydberg states to form the molecular ion HCl^+, followed by (ii) a second one-photon excitation to a repulsive ion state ($(2)^2\Pi$) and dissociation [see Figs. 1(a) and 1(b)] to form H^+. HCl^+ could be formed partly by direct ionization and partly by autoionization.[19]

(2) Several ionization channels, via the noncoupled (diabatic) ion-pair state, have been proposed,[19–22] involving (iii) one-photon autoionization via a repulsive superexcited state which correlates with $H+Cl^*$ to form HCl^+ largely in high vibrational (v^+) levels,[19] followed by (iv) a second one-photon excitation to a repulsive ion state ($(2)^2\Pi$) and dissociation (analogous to ii), (v) one-photon excitation to repulsive triplet superexcited states,[20,21] forming H and Cl^* ($Cl^*=Cl^*(4s,4p,3d)$), followed by one-photon ionization of Cl^* to form Cl^+, (vi) one-photon excitation to a repulsive superexcited state (HCl^*, $^1\Sigma^+$), forming $H^*(n=2)$ and $Cl(^2P_{1/2})$, followed by one-photon ionization of $H^*(n=2)$ to form H^+, and (vii) one-photon excitation to a bound superexcited state ($[A\,^2\Sigma^+]^1\Sigma^+$), which acts as a gateway state to dissociation into the ion-pair $H^+ + Cl^-$.[22] The last channel was found to be $V\,^1\Sigma^+$-vibrational-state selected. More channels have been proposed[20,22] via the

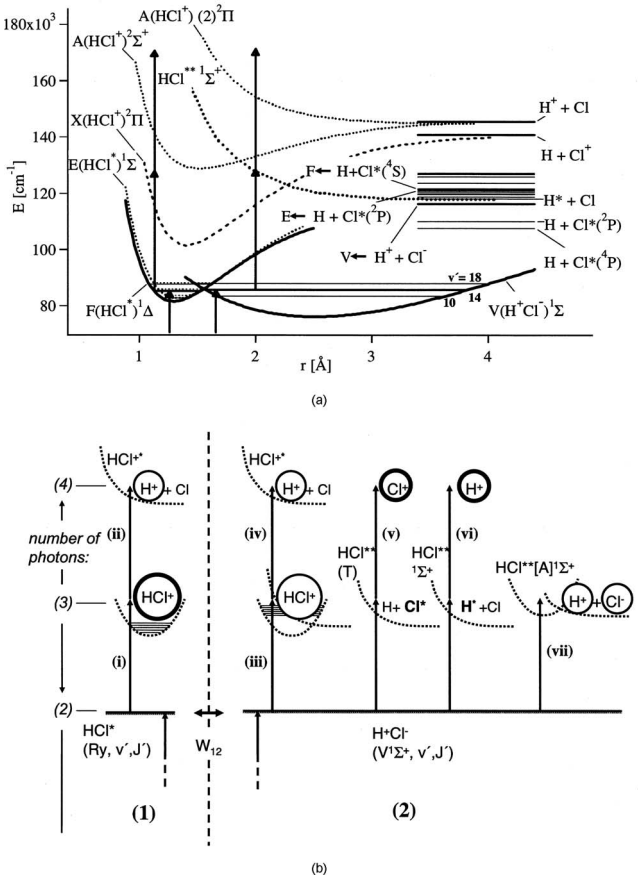

FIG. 1. HCl energetics. (a) Potential energy curves, asymptotic energies (right), and vibrational levels in the Rydberg states $F\,^1\Delta_2$ and $E\,^1\Sigma^+(v'=0-2)$ and in the $V\,^1\Sigma^+$ ion-pair state ($v'=10$, 14, and 18). The potential curves for the F and V states are Morse potentials (solid curves) derived from experimental data in Refs. 6 and 14 ($F\,^1\Delta_2$) and 6 and 52 ($V\,^1\Sigma^+$). Other potential curves (dotted curves) are based on theoretical calculations in Ref. 27 (E state) and 29 (ion states and superexcited state (HCl^{**})). The arrows represent excitations relevant to ($2+n$; $n=1,2$) REMPI via the $F\,^1\Delta_2(v'=1)$ (left) and the $V\,^1\Sigma^+(v'=14)$ states. (b) Schematic diagram showing major ionization channels following excitations (1) to diabatic Rydberg states [left of vertical broken line; channels (i) and (ii)] and (2) to a hypothetical diabatic $V\,^1\Sigma^+$ ion-pair state [right of vertical broken line; channels (iii) and (vii)]. The arrows represent excitations relevant to ($2+n$; $n=1,2$) REMPI. Fragment and excited state species are indicated. Ions formed are highlighted with circles. Main ion formations (HCl^+, H^+, and Cl^+) are indicated with bold circles. Total number of photons is indicated to the left. See text for further clarification.

noncoupled ion-pair state, but these are believed to be of minor importance.

Thus, based on this overall ionization scheme, Cl^+ (and Cl^-) are characteristic indicators for the ion-pair state contribution. H^+ formation clearly is both indicative of the ion pair and the Rydberg state contribution. However, its major formation pathway is found to be the fragmentation channel (vi) indicative of excitation to the ion-pair state. HCl^+ formation is the main ion formation channel via Rydberg state excitation [channel (i)] under low power conditions. There are reasons to believe that the HCl^+ contribution to ion formation, via excitation to the V state, is rather small. For example, de Beer *et al.* have shown that the main source of photoelectrons arising from excitation of the $v=9$ level of the V state is the photoionization of the excited hydrogen and chlorine atoms[10] and Green and Wallace have observed a large contribution of the photofragmentation channels upon excitation of the E and V states.[9] Furthermore, Chichinin *et al.* found rather limited contribution of HCl^+ in high v^+ levels for excitations via the V state, $v'=12$. Hence we believe that the HCl^+ formation is mainly an indicator for the Rydberg state contribution.

In this paper, we use a two-dimensional (2D) REMPI approach, obtained by recording ion-mass spectra as a function of the laser frequency, to study the photorupture dynamics of HCl for two-photon resonance excitations via the $F\,^1\Delta_2$ Rydberg state and the $V\,^1\Sigma^+$ ion-pair state. Quantum level dependent ion-signal intensities, consistent with near-resonance couplings, are observed for $H^{35}Cl$ and $H^{37}Cl$. Coupling strengths W_{12} can be derived from signal intensity and line shift analysis. Proposed mechanisms for resonance diabatic Rydberg state excitations are supported by ion-signal power dependence studies. Furthermore, we calculated potential energy curves relevant to the above-mentioned processes by various *ab initio* methods and performed comparisons with experimental data and calculations by others. We carried the theoretical treatment a step further and evaluated v'-dependent rotational constants and calculated the corresponding "*ab initio* REMPI spectra" for comparison with the experimental data.

EXPERIMENTAL

REMPI of jet cooled HCl gas was performed. Ions were directed into a time-of-flight tube and detected by a microchannel plate (MCP) detector to record the ion yield as a function of mass and laser radiation wavenumber to obtain 2D REMPI data.

The apparatus used is similar to that described elsewhere.[16,35] Tunable excitation radiation in the 227–242 nm wavelength region was generated by excimer laser-pumped dye laser systems, using a Lambda Physik COMPex 205 excimer laser, either with a Lumonics Hyperdye 300 or a Coherent ScanMatePro dye laser. Relevant dyes were used and frequency doubling obtained with BBO-B or BBO-2 crystals. The repetition rate was typically 5 or 10 Hz. The bandwidths of the dye laser beam were about 0.05 cm^{-1} for Lumonics Hyperdye 300 and about 0.095 cm^{-1} for Coherent ScanMatePro. Typical laser intensity used was 0.2 mJ/pulse. The radiation was focused into an ionization chamber between a repeller and an extractor plate. We operated the jet in conditions that limited cooling in order not to lose transitions from high rotational levels. Thus, an undiluted, pure HCl gas sample (Merck-Schuchardt OHG; purity >99.5%) was used. It was pumped through a 500 μm pulsed nozzle from a typical total backing pressure of about 1.0–1.5 bars into the ionization chamber. The pressure in the ionization chamber was lower than 10^{-6} mbar during experiments. The nozzle was kept open for about 200 μs and the laser beam was typically fired 500 μs after opening the nozzle. Ions were extracted into a time-of-flight tube and focused onto a MCP detector, of which the signal was fed into a LeCroy 9310A, 400 MHz storage oscilloscope as a function of flight time. Average signal levels were evaluated and recorded for a fixed number of laser pulses to obtain the mass spectra. Mass spectra were typically recorded in 0.05 or 0.1 cm^{-1} laser wavenumber steps. Spectral points were generally obtained by averaging over 100 pulses. The power dependence of the ion signal was determined by integrating the mass signals repeatedly and averaging over approximately 1000 pulses, after bypassing different numbers of quartz windows to reduce power. Care was taken to prevent saturation effects as well as power broadening by minimizing laser power. Wavelength calibration was achieved by recording iodine atomic lines[36] and by the strongest hydrogen chloride rotational lines reported by Green *et al.*[8] The accuracy of the calibration was found to be about ± 1.0 cm^{-1} on a two-photon wavenumber scale. Intensity drifts during the scan were taken into account, and spectral intensities were corrected for accordingly.

RESULTS AND ANALYSIS

2D REMPI

Figures 2(a) and 2(b) show 2D REMPI data for HCl ($H^{35}Cl:H^{37}Cl \sim 3:1$) in the two-photon excitation region of 85 300–85 700 cm^{-1}. Contour plots are shown below, and REMPI spectra for different ion masses, as well as for total mass signals are shown above. The REMPI spectra for individual ions were obtained by integrating signal intensities for narrow time-of-flight (hence mass) ranges such as that marked by the squared area in the lower part of Fig. 2(b) for $H^{35}Cl^+$. Figure 2(b) shows the Q branch rotational lines for $J=2-9$, $F\,^1\Delta_2(v'=1) \leftarrow\leftarrow X\,^1\Sigma^+(v'=0)$ and for $J'=8$, $V\,^1\Sigma^+(v'=14) \leftarrow\leftarrow X\,^1\Sigma^+(v'=0)$ in the 85 320–85 365 cm^{-1} excitation energy region. Rotational transitions due to the $F\,^1\Delta_2(v'=1) \leftarrow\leftarrow X\,^1\Sigma^+(v'=0)$ and $V\,^1\Sigma^+(v'=14) \leftarrow\leftarrow X\,^1\Sigma^+(v'=0)$ transitions have been identified and assigned. H^+ signals are observed for all resonance transitions involved. $H^{35}Cl^+$ and $H^{37}Cl^+$ ions are detected for all transitions within $H^{35}Cl$ and $H^{37}Cl$, respectively, whereas $^{35}Cl^+$ and $^{37}Cl^+$ ions are observed for all $V \leftarrow\leftarrow X$ transitions but only for transitions to $J'=8$ in $F\,^1\Delta_2(v'=1)$ within $H^{35}Cl$ and $H^{37}Cl$, respectively [see Fig. 2(b)]. This observation for the $V \leftarrow\leftarrow X$ resonance transitions is in agreement with expectations, since the V state couples to a number of Rydberg

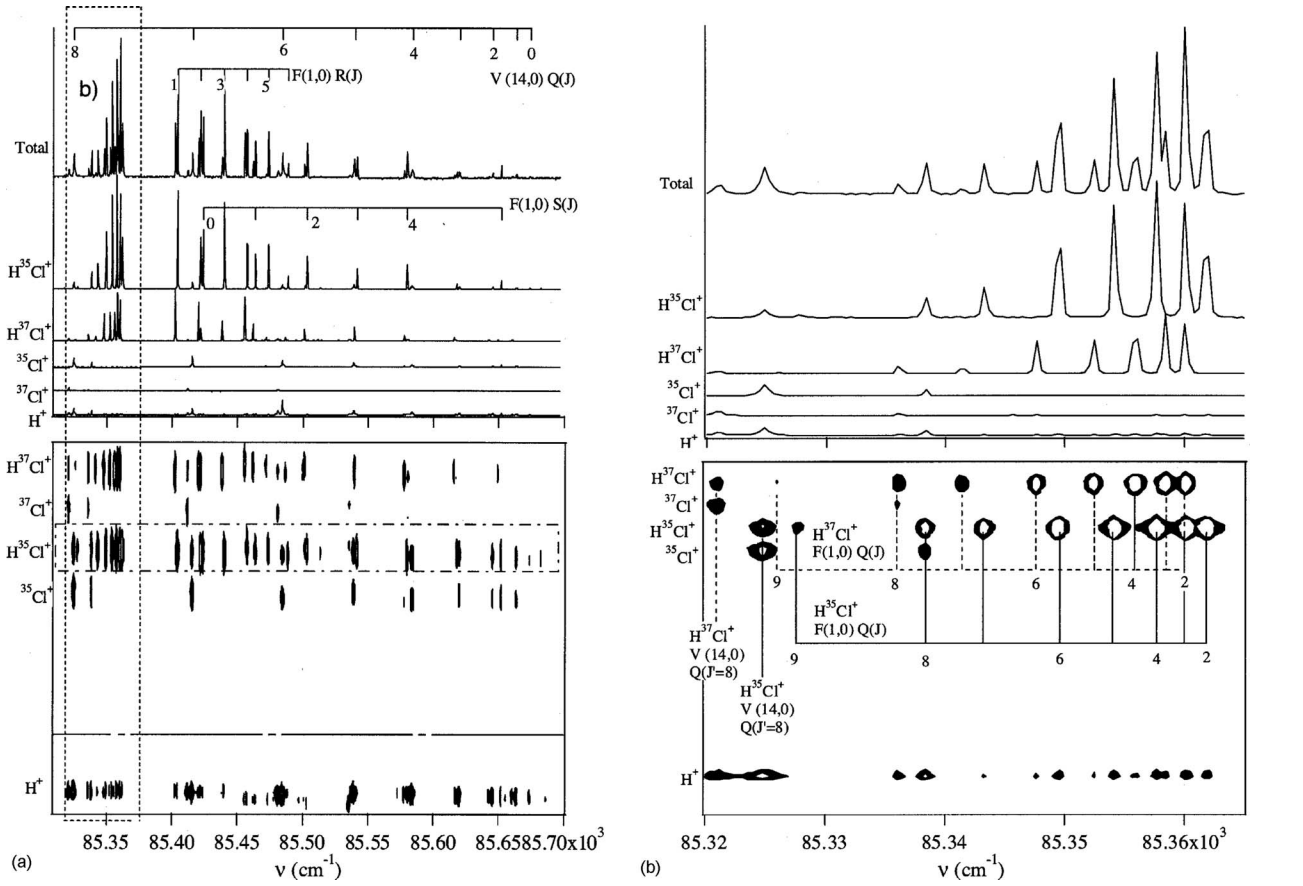

FIG. 2. 2D REMPI contours (below) and REMPI spectra (above) for H^+, $^{35}Cl^+$, $H^{35}Cl^+$, $^{37}Cl^+$, and $H^{37}Cl^+$ derived from HCl with isotope ratios in natural abundance. $J=J''$ in the figures. (a) Excitation region of 85 300–85 700 cm^{-1}. Assignments for R and S rotational lines for $F\,^1\Delta_2(v'=1)\leftarrow\leftarrow X\,^1\Sigma^+(v''=0)$ ($H^{35}Cl$) and for Q rotational lines for $V\,^1\Sigma^+(v'=14)\leftarrow\leftarrow X\,^1\Sigma^+(v''=0)$ ($H^{35}Cl$) transitions are shown. (b) Excitation region of 85 320–85 365 cm^{-1}. Assignments for Q rotational lines for $F\,^1\Delta_2(v'=1)\leftarrow\leftarrow X\,^1\Sigma^+(v''=0)$ ($H^{35}Cl$ and $H^{37}Cl$) and for Q rotational lines for $V\,^1\Sigma^+(v'=14)\leftarrow\leftarrow X\,^1\Sigma^+(v''=0)$ ($J'=8$; $H^{35}Cl$ and $H^{37}Cl$) transitions are shown.

states and will therefore show ion formations according to all channels (i)–(vii), mentioned above and shown in Fig. 1(b). The lack of Cl^+ ions for all resonance transitions except to $v'=1$, $J'=8$ in the F state suggests that negligible coupling to the V state occurs for these states and that the ionization follows channel (1) [i.e., (i) and (ii) in Fig. 1(b)]. The observed Cl^+ signals for resonance excitations to $F\,^1\Delta_2(v'=1)$, $J'=8$ both for $H^{35}Cl$ and $H^{37}Cl$ are consistent with a near-resonance interaction, $F\,^1\Delta_2(v'=1)$, $J'=8\leftrightarrow V\,^1\Sigma^+(v'=14)$, $J'=8$ in agreement with earlier reported data on line shift analysis for $H^{35}Cl$.[14]

For convenience and to help with interpretations we evaluated normalized ion-signal intensities ($I_N(M^+)$) defined in the following way: Ion intensities ($I(M^+)$) detected via Rydberg state excitations were normalized with respect to the HCl^+ ion intensities [the main Rydberg state indicator, $I(HCl^+)$] to obtain $[I_N(M^+)]_{Ry}=[I(M^+)/I(HCl^+)]_{Ry}$. Ion intensities detected via the V ion-pair state excitations were normalized with respect to the Cl^+ ion intensities [the V ion-pair state indicator, $I(Cl^+)$] to obtain $[I_N(M^+)]_v=[I(M^+)/I(HCl^+)]_v$. Figures 3(a)–3(d) show normalized ion intensities for $H^{35}Cl$ and $H^{37}Cl$ for various resonance excitations derived for constant laser power. Figure 3(a) shows that not only do Cl^+ ions appear, following resonance excitations to $F\,^1\Delta_2(v'=1)$, $J'=8$, but H^+ ion signals are also found to be enhanced with respect to HCl^+ (i.e., the main Rydberg state indicator) for resonance excitations to $F\,^1\Delta_2(v'=1)$, $J'=8$ compared to $J'\neq 8$. This is due to opening up of the H^+ excitation channels (iv), (vi), and (vii) via $V\,^1\Sigma^+(v'=14)$, $J'=8$, of which channel (vi) is believed to be the largest.[22] Judging from normalized HCl^+ signals for $V\,^1\Sigma^+(v'=14)$, $J'=0$–9 [see Fig. 3(b)], HCl^+ ion formation also is enhanced for resonance excitations to $V\,^1\Sigma^+(v'=14)$, $J'=8$. This is a further indication of the resonance coupling from the V state side. The relatively large enhancement in the HCl^+ signal is an additional indication (see previous arguments) that HCl^+ is a major indicator for the Rydberg state contribution. The significantly lower relative signals for $H^{37}Cl$ compared to $H^{35}Cl$, shown in both Figs. 3(a) and 3(b), indicate smaller resonance coupling in the former case. The overall drops in the relative signal strengths observed for $V\,^1\Sigma^+(v'=14)\leftarrow\leftarrow X\,^1\Sigma^+(v'=0)$ [Fig. 3(b)] with increasing J' for $J'>2$ is due to decreasing nonresonance couplings between V ($v'=14$) and other Rydberg states, of which the coupling to the $E(v'=1)$ state plays the major role. An analogous effect is observed for the $E\,^1\Sigma^+(v'=1)\leftarrow\leftarrow X\,^1\Sigma^+(v'=0)$ transition, i.e., decreasing $I(Cl^+)/I(HCl^+)$ and $I(H^+)/I(HCl^+)$ ratios, hence decreasing coupling strength as J' increases ($J'>1$) [see Fig. 3(c)].

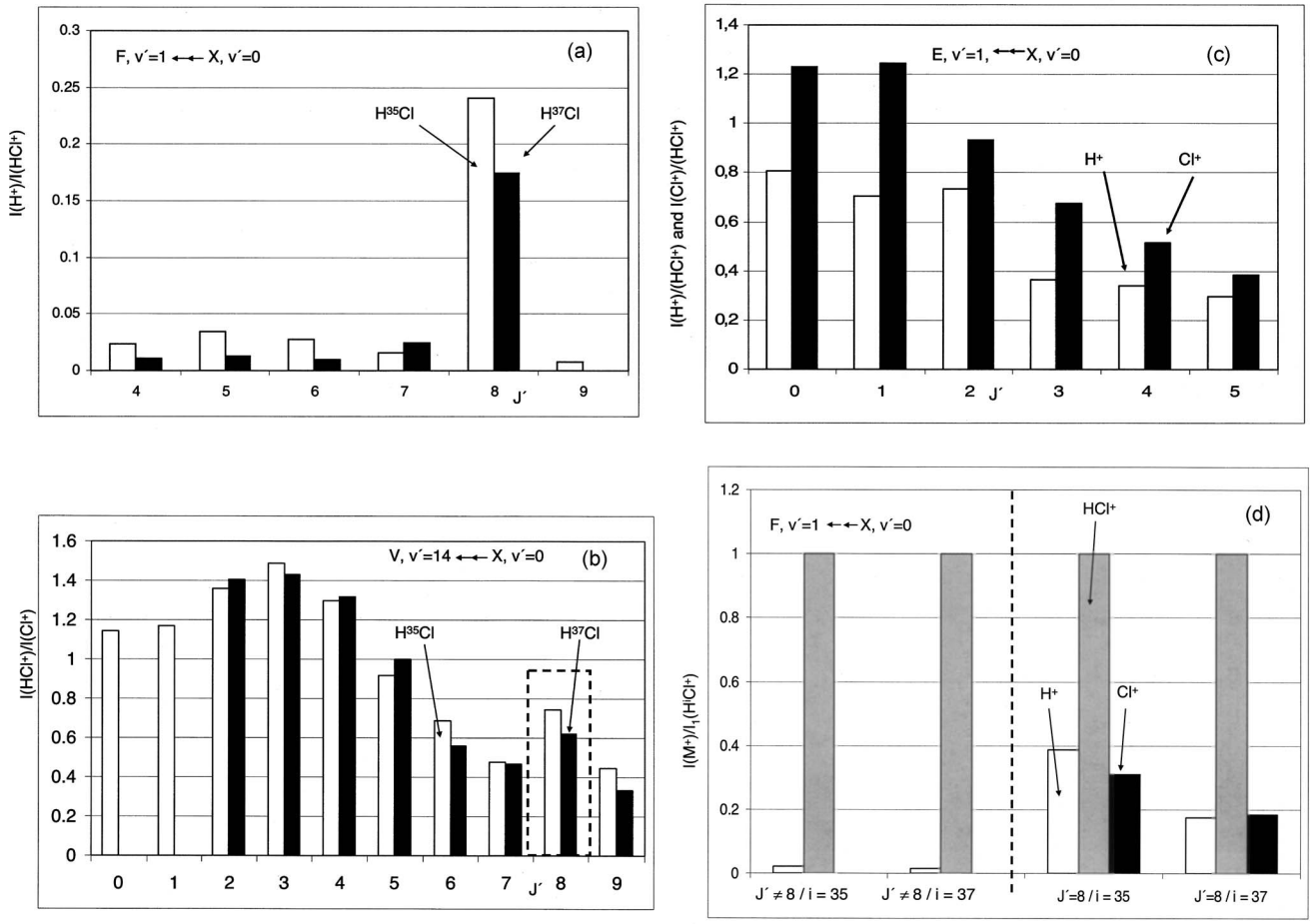

FIG. 3. Relative/normalized ion-mass signals. (a) $I(H^+)/I(HCl^+)$ for $H^{35}Cl$ and $H^{37}Cl$, in the case of ionization via the Rydberg state (1) $F\,^1\Delta_2(v'=1)$ as a function of J'; $J'=4-9$. (b) $I(HCl^+)/I(Cl^+)$ for $H\,^{35}Cl$ and $H^{37}Cl$ in the case of ionization via the ion-pair state (2) $V\,^1\Sigma^+(v'=14)$ as a function of J'; $J'=0-9$. (c) $I(H^+)/I(HCl^+)$ and $I(Cl^+)/I(HCl^+)$ for $H^{35}Cl$ in the case of ionization via the Rydberg state (1) $E\,^1\Sigma^+(v'=1)$ as a function of J'; $J'=0-5$. (d) ion-mass signals normalized with respect to $I(HCl^+)$/the $F(1)$ state indicator $(I(M^+)/I(HCl^+))_1$; $M^+=H^+$, Cl^+, and HCl^+ for $H^{35}Cl$ and $H^{37}Cl$, in the case of ionization via the Rydberg state (1) $F\,^1\Delta_2(v'=1)$, $J'=8$ (on right side of the broken vertical line) and for $J'\neq 8$ (average of data for $J'=4-7$) (on left side of the broken vertical line).

Laser power dependence vs excitation mechanisms

Ion intensities ($I(M^+)$) and intensity ratios ($I(M^+)/I(N^+)$) vary with laser power (P_{laser}) depending on the number of photons needed to ionize $(n,m,\ldots)$ and on the transition probabilities

$$I(M^+) = C' P_{laser}{}^n, \tag{1}$$

C' is proportionality constant depending on the transition probability. Based on Eq. (1) the following expressions can be derived:

$$\log I(M^+) = n \log P_{laser}^{ref} + C \tag{2a}$$

and

$$\log I(M^+)/I(N^+) = (n-m)\log P_{laser}^{ref}, \tag{2b}$$

where P_{laser}^{rel} is proportional to the laser power. This permits easy extraction of photon numbers or photon number differences $(n-m)$ for ionization processes from the slopes in relevant log-log plots.

Assuming that H^+ and HCl^+ ion signals, formed via resonance excitation to a noncoupled Rydberg state, follow channel (1) [Fig. 1(b)], the sum of the H^+ and HCl^+ signals will be a measure of the HCl^+ ion formation, whereas the H^+ formation is found by direct measurement of H^+ signals. Figure 4(a) shows typical log-log plots relevant to testing these criteria for the H^+ and HCl^+ ion formation obtained for resonance excitations via rotational levels other than $J'=8$, $v'=1$ in the F state [i.e., for ionizations via noncoupled (diabatic) Rydberg states]. Based on slope evaluations, the numbers of excitation photons for HCl^+ and H^+ formations are indeed found to be 3 and 4, respectively, in agreement with the model as presented in Fig. 1(b).

Figure 4(b) shows log-log plots derived from a resonance excitation to the coupled Rydberg state $F\,^1\Delta_2(v'=1)$, $J'=8(\leftrightarrow V\,^1\Sigma^+(v'=14), J'=8)$ by tuning to the S(6) rotational line [excitation from $X\,^1\Sigma^+(v'=0)$, $J'=6$], using minimum possible laser power. Assuming the ionization to follow both channels (1) and (2) [Fig. 1(b)], $I(H^{35}Cl^+)$ will increase with power cubed in the low power limit [assuming negligible H^+ to be formed by channel (ii)], in agreement with the observation. Based on the work of Romanescu and Loock,[11,22] who observed maximum contribution to the H^+ formation by channel (v) (three-photon ionization) for $v'=12$ and gradually lower contribution as v' increased from 12 to 15, a minor contribution from channel (v) is to be

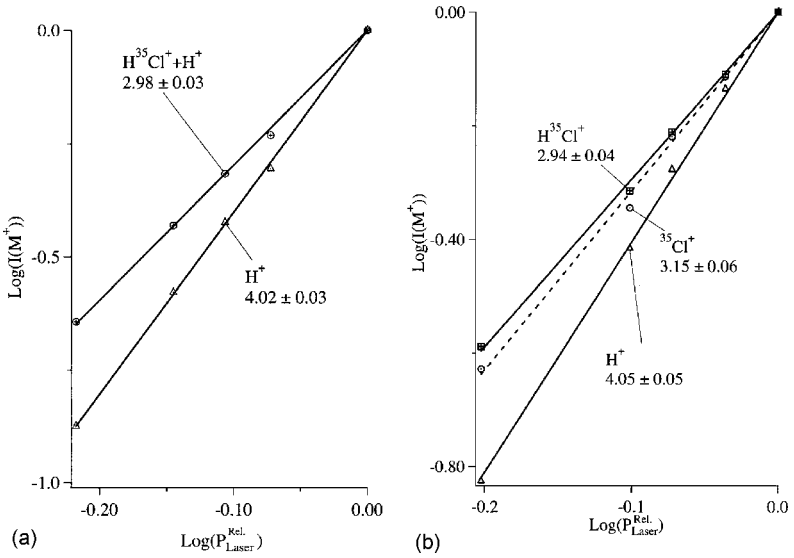

FIG. 4. Number of photons needed for ionization processes. (a) $\log(I(H^{35}Cl^+)+I(H^+))$ and $\log(I(H^+))$ vs $\log(P^{rel}_{laser})$ for ionization via the resonance excitation $F\,^1\Delta_2(v'=1;J'=4)\leftarrow\leftarrow X\,^1\Sigma^+(v''=0;J''=3)/R(J'=4)$ rotational line. The numbers of photons needed for $H^{35}Cl^+$ and H^+ formations are determined from the slopes (indicated) as 3 and 4, respectively. See text for further clarification. (b) $\log(I(H^{35}Cl^+))$, $\log(I(H^+))$, and $\log(I(^{35}Cl^+))$, vs $\log(P^{rel}_{laser})$ for ionization via the resonance excitation $F\,^1\Delta_2(v'=1;J'=8)\leftarrow\leftarrow X\,^1\Sigma^+(v''=0;J''=6)/S(J'=8)$ rotational line. See text for further clarification. Ion intensities are normalized to $I(M^+)=1$ for $P^{rel}_{laser}=1$.

expected for $v'=14$, whereas the major contribution to the H^+ formation is expected to be by the four-photon ionization channel (iii). This is consistent with the observed "photon number value/n" of 3.82 ± 0.6 for $I(H^+)$. The reproducible observation of $n\approx3$ for Cl^+ formation, however, came as a surprise. As seen in Fig. 1(a), the lowest energy limit for Cl^+ formation via a $F\,^1\Delta_2(v'=1)$ excitation requires a minimum of four photons. A possible explanation for an observed photon number value lower than four could be that the chlorine ionization occurs via formation of the short-lived $Cl^*(4s)$ species (τ=2.0 ns),[20] in which case spontaneous decay will compete with laser excitation which occurs within the approximately 10 ns of the laser pulse duration.

State interactions and contributions vs excitation mechanisms

The resonance coupling strengths for $H^{35}Cl$ and $H^{37}Cl$ between the F and V states $(F\,^1\Delta_2(v'=1),J'=8\leftrightarrow V\,^1\Sigma^+(v'=14),J'=8)$ could be estimated from relevant rotational line positions combined with estimates of mixing fractions from ion-signal intensities in the following way. Level to level interactions are represented by

$$E_i=\tfrac{1}{2}(E_1^0+E_2^0)\pm\tfrac{1}{2}[4|W_{12}|^2+(E_1^0-E_2^0)^2]^{1/2}, \tag{3}$$

where E_1^0 and E_2^0 are the zero-order rovibrational level energies for the unperturbed states 1 and 2 and W_{12} is the matrix element of the perturbation function/interaction strength.[37] E_1 and E_2 are the resulting level energies of the perturbed states (for the high and low energy states, respectively). The eigenfunctions of the perturbed levels (ψ_1 and ψ_2) are related to the eigenfunctions of the unperturbed states (ψ_1^o and ψ_2^o) as

$$\psi_1=c_1\psi_1^o-c_2\psi_2^o,$$

$$\psi_2=c_1\psi_1^o+c_2\psi_2^o, \tag{4}$$

where, for normalized wavefunctions and $\Delta E=E_1-E_2$,

$$c_i^2=\frac{1}{2}\pm\frac{\sqrt{|\Delta E|^2-4|W_{12}|^2}}{2|\Delta E|} \tag{5a}$$

are weight factors for the state mixing. Since rotational lines which belong to the same branch $(X=O,P,Q,R,S)$ for mixing states (equal J quantum numbers) are due to transitions from the same initial state, E_1 and E_2 can be replaced with the corresponding transition energies (or wavenumbers) $\tilde{\nu}_1(X)$ and $\tilde{\nu}_2(X)$ [and ΔE can be replaced with $\Delta\tilde{\nu}=\tilde{\nu}_1(X)-\tilde{\nu}_2(X)$],

$$c_i^2=\frac{1}{2}\pm\frac{\sqrt{|\Delta\tilde{\nu}|^2-4|W_{12}|^2}}{2|\Delta\tilde{\nu}|}. \tag{5b}$$

The wavenumber differences for transitions to the two states (1) $F\,^1\Delta_2(v'=1)$, $J'=8$ and (2) $V\,^1\Sigma^+(v'=14)$, $J'=8$, for the same rotational branches X $((\tilde{\nu}_1(X,J'=8)-\tilde{\nu}_2(X,J'=8))=|\Delta\tilde{\nu}_{J'=8}|=|\Delta E_{J'=8}|)$ for $H^{35}Cl$ and $H^{37}Cl$ [see, for example, Fig. 2(b) for the Q branch] were found to be on average,

$$H^{35}Cl:\quad \tilde{\nu}_1(Q,J'=8)-\tilde{\nu}_2(Q,J'=8)$$
$$=|\Delta\tilde{\nu}_{J'=8}|=|\Delta E_{J'=8}|=11.3\ \text{cm}^{-1},$$

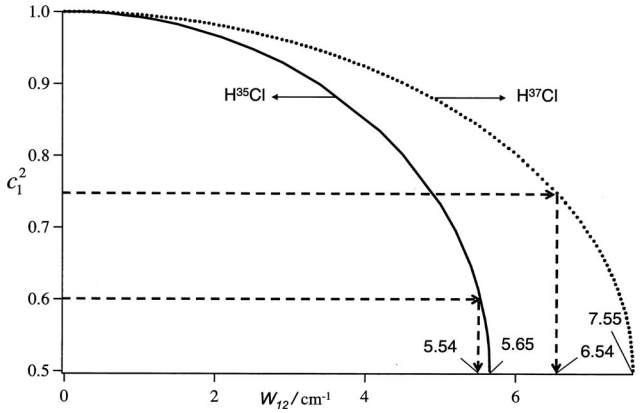

FIG. 5. Weight factors c_1^2 as a function of interaction strength (W_{12}) for the $F\,^1\Delta_2(v'=1;J'=8)$ (1) state in the $F\,^1\Delta_2(v'=1;J'=8)(1)\leftrightarrow V\,^1\Sigma^+(v'=14;J'=8)(2)$ state mixing for $H^{35}Cl$ (solid curve) and $H^{37}Cl$ (dotted curve) derived from Eqs. (5a) and (5b) and the spacing between corresponding Q branch lines.

$$H^{37}Cl: \quad \tilde{v}_1(Q,J'=8)-\tilde{v}_2(Q,J'=8)$$
$$=|\Delta\tilde{v}_{J'=8}|=|\Delta E_{J'=8}|=15.1\ \text{cm}^{-1}.$$

Therefore the fractional contributions c_1^2 (corresponding to the high energy state) according to Eqs. (5a) and (5b) vary with $|W_{12}|$ for $0.5<c_1^2<1$, as shown in Fig. 5. This gives upper limits to the interaction strength, corresponding to a resonance interaction (i.e., $E_1^0=E_2^0$) and $c_1^2=0.5$,[37] $|W_{12}^{\max}|$,

$$|W_{12}^{\max}|=\frac{|\Delta E_{J'=8}|}{2}=\frac{|\Delta\tilde{v}_{J'=8}|}{2} \tag{6}$$

as 5.65 and 7.55 cm^{-1} for $H^{35}Cl$ and $H^{37}Cl$, respectively, in the case of the $F\ ^1\Delta_2(v'=1)$, $J'=8\leftrightarrow V\ ^1\Sigma^+(v'=14)$, $J'=8$ interaction.

Based on Eqs. (5a) and (5b) the actual interaction strength ($|W_{12}|$) could be evaluated if the weight factor c_1^2 for the F state in the $F\leftrightarrow V$ mixing ($v'=1$, $J'=8$) (hence the weight factor for the V state, $c_2^2=1-c_1^2$) was known,

$$|W_{12}|=|\Delta E_{J'=8}|\sqrt{1-4[c_1^2-1/2]^2}/2$$
$$=|\Delta\tilde{v}_{J'=8}|\sqrt{1-4[c_1^2-1/2]^2}/2. \tag{7}$$

As an attempt to estimate c_1^2 we made use of the ion signals as follows. The basic assumption is made that c_1^2 is equal to the sum of all normalized ion signals formed via the noncoupled (diabatic) $F(1)$-state excitation ($\Sigma_i[I_N(M_i^+)]_{\text{nc}}$) divided by the total normalized ion signal formed via the F-state excitations in the coupled (adiabatic) state (F, $v'=1$, $J'=8$) ($\Sigma_j[I_N(M_j^+)]_{\text{c}}$),

$$c_1^2=\frac{\Sigma_i[I_N(M_i^+)]_{\text{nc}}}{\Sigma_j[I_N(M_j^+)]_{\text{c}}}. \tag{8}$$

As an approximation to represent $\Sigma_i[I_N(M_i^+)]_{\text{nc}}$ we used the averaged sum of normalized ion signals for ionizations via rotational levels in the F state close to $v'=1$, $J'=8$ [see $J'=4-7$ and 9 in Fig. 3(a)], i.e., $\Sigma_i[I_N(M_i^+)]_{J'\neq 8}$, where insignificant coupling was observed [see Fig. 3(d)]. $\Sigma_j[I_N(M_j^+)]_{\text{c}}$ was taken to be the sum of the normalized ion signals for $v'=1$, $J'=8$ [i.e., $\Sigma_j[I_N(M_j^+)]_{J'=8}$]. Therefore, since normalized ion intensities for HCl^+ are equal to 1, c_1^2 is

$$c_1^2=\frac{([I_N(H^+)]_{J\neq 8}+1)}{([I_N(H^+)]_{J'=8}+[I_N(Cl^+)]_{J'=8}+1)}. \tag{9}$$

Thus $c_1^2=0.60$ and 0.75 were obtained for $H^{35}Cl$ and $H^{37}Cl$, respectively, which gives $|W_{12}|\cong 5.54$ and 6.54 cm^{-1} for $H^{35}Cl$ and $H^{37}Cl$, respectively (see Fig. 5 and Table I). Notice that this assumes that the ion signals HCl^+ and Cl^+ for $F\ ^1\Delta_2$ ($v'=1$), $J'=8$ originate from ionizations of the diabatic $F(1)$ and $V(2)$ states, respectively, whereas the H^+ signal originates from both sources according to the ionization procedure above, and presented in Fig. 1(b). As mentioned before, a small contribution to HCl^+ formation due to excitation via the V state cannot be excluded, which makes the c_1^2 estimated values ($c_1^2=0.60$ and 0.75) upper limit values, hence the $|W_{12}|$ values (5.54 and 6.54 cm^{-1}) lower limit values. $5.54\sim<|W_{12}|<5.64\ \text{cm}^{-1}$ ($|W_{12}^{\max}|$) obtained for $H^{35}Cl$ is in good agreement with the value, $6\pm 2\ \text{cm}^{-1}$, obtained solely from relative shifts of rotational lines in the $F\ ^1\Delta_2(v'=1)\leftarrow\leftarrow X\ ^1\Sigma^+(v'=0)$ spectrum for $H^{35}Cl$.[14]

TABLE I. $H^{35}Cl$: Spacings between observed rotational energy levels ($\Delta E=E_1-E_2$) (=spacings between transitions of same rotational branches, X ($\Delta v=\tilde{v}_1(X)-\tilde{v}_2(X)$) in the $F\ ^1\Delta_2(v'=1,J')$ and the $V\ ^1\Sigma^+(v'=14;J')$ states for equal J' values, coupling strengths as a function of $J'(|W_{12}|)$, and fractional population in the state $F\ ^1\Delta_2(v'=1,J')$ (1) (c_1^2).

J'	$\lvert\Delta E\rvert/\lvert\Delta\tilde{v}\rvert$ (cm^{-1})	$\lvert W_{12}\rvert$[a] (cm^{-1})	c_1^2[b]
2	282.9	1.60	1.00
3	256.8	2.28	1.00
4	224.4	2.92	1.00
5	185.2	3.58	1.00
6	134.2	4.23	1.00
7	70.6	4.89	0.99
8	11.3	5.54	0.60
9	105.6	6.19	0.99

[a]From Eq. (10) for $W_{12}'=0.653\ \text{cm}^{-1}$ (see text).
[b]Equations (5a) and (5b).

It has been argued that the $F\ ^1\Delta$ state wave function may be a linear combination of $\Omega=1-3$ components, in which case the weak perturbation observed is probably due to a heterogeneous ($\Delta\Omega>0$) coupling.[11,14] Hence $|W_{12}|$ will be proportional to the square root of $J'(J'+1)$,[38]

$$|W_{12}|=W_{12}'(J'(J'+1))^{1/2} \tag{10}$$

and $W_{12}'\sim 0.653$ and 0.771 cm^{-1} for $H^{35}Cl$ and $H^{37}Cl$, respectively, derived from the approximate $|W_{12}|$ values for $J'=8$. This allows determination of $|W_{12}|$ and c_1^2 [Eqs. (5a) and (5b)] values for $J'\neq 8$ (see Table I for $H^{35}Cl$, $J'=2-7$ and 9). Notice that the weight factors c_1^2 for $J'\neq 8$ are very close to unity (hence $c_2^2\approx 0$, i.e., negligible V-state contribution), which makes it understandable why insignificant ionization via the $V\ ^1\Sigma^+$ state is observed in those cases.

Potential energy curves and *ab initio* REMPI spectra

Major perturbation effects observed in singlet excited states of HCl are found to be due to interactions between Rydberg states and the $V\ ^1\Sigma^+$ ($\Omega=0$) ion-pair state. Some less obvious mixing between Rydberg states has also been predicted or observed indirectly.[3,11] A rule of thumb is that state interactions decrease as symmetry differences between states increase, and with increasing differences between electronic spin and orbital angular momentum quantum numbers. Thus there is a reason to believe that an *ab initio* potential energy curve for the lowest energy singlet delta excited state ($\Omega=2$) could be used to reproduce the experimental data without taking into account state interactions, since the weak mixing is only observed for the $v'=1$, $J'=8$ state.

Various *ab initio* calculations [DFT and time-dependent DFT with the B3LYP and the MPW1PW91 functionals, MP2, MP4, CC and EOM-CC and completely renormalized coupled cluster (CR-EOM-CC) calculations] were performed on the singlet states of HCl, and potential energy curves and spectroscopic parameters were derived for the ground state and the lowest energy $\triangle$ state. The REMPI spectra for the corresponding transitions were also evaluated. Potential en-

ergy curves were determined using the GAUSSIAN03,[39] the NWCHEM,[40] and the ACESII[41] program packages. A restricted Hartree–Fock wavefunction was employed as a reference function in the MP and CC calculations, with all electrons being correlated. CCSD and CCSD(T) calculations were carried out for the ground state and both EOM-CCSD[42] and CR-EOM-CCSD(T)[43] calculations were used for excited states. The augmented correlation consistent basis sets by Dunning *et al.* aug-cc-pVnZ (n=T,Q,5),[44] and its core-valence versions aug-cc-pCVnZ (n=T,Q),[45] were employed as obtained from the basis set exchange.[46] Additionally, the aug-cc-pVQZ basis set was further augmented by adding 3s, 3p, 2d, and 1f diffuse functions for H (exponents in atomic units of 0.023 630, 0.006 211, 0.000 146, 0.084 800, 0.024 626, 0.002 088, 0.190 000, 0.054 531, 0.136 800, respectively), and 3s, 3p, 2d, 2f, and 2g functions for Cl (exponents of 0.051 900, 0.018 823, 0.006 827, 0.037 600, 0.013 337, 0.004 813, 0.095 200, 0.035 681, 0.217 000, 0.082 460, 0.378 000, 0.143 640, respectively), to give the basis set referred to as AQZ. Ground-state potential energy curves and lowest energy potential energy curves for delta orbital symmetry ($^1\Delta$ states) were fitted by Morse potential functions ($U(r)$) to determine average internuclear distances [r_e (Å)], dissociation energies [D_e (cm^{-1})], vibrational frequencies [ω_e (cm^{-1})], anharmonicity parameters [$\omega_e x_e$ (cm^{-1})], and the rotational parameter B_e (cm^{-1}),

$$U(r) = T_0 + D_e\{1 - \exp(-\beta(r - r_e))\}^2, \tag{11a}$$

$$\omega_e = \left(\beta\sqrt{\frac{D_e}{\mu}}\right) \Big/ 0.121\,77,$$

$$\omega_e x_e = \omega_e^2/(4D_e), \quad B_e = \frac{h^2}{8\pi^2\mu r_e^2}, \tag{11b}$$

for T_0 in cm^{-1}, μ in g mol^{-1}, and β in Å^{-1}. The nuclear Schrödinger equation was solved numerically on the Morse potentials to evaluate vibrational wavefunctions (ψ_v) and obtain averaged internuclear distances ($\langle r_v\rangle$) and corresponding first and second order rotational parameters B_v and D_v as a function of vibrational quantum number,

$$\langle r_v\rangle = \int_0^\infty r\psi_v^2 dr, \quad B_v = \frac{h^2}{8\pi^2\mu\langle r_v\rangle^2}, \quad D_v = 4B_v^3/\omega_e^2. \tag{12}$$

Finally, two-photon absorption spectra were calculated as has previously been described.[13–15,17] Thus rotational line positions were derived from the expression

$$\tilde{\upsilon}_{J',v'\leftarrow J'',v''} = \tilde{\upsilon}^0_{v'\leftarrow v''} + \Delta E_{J',J''}, \tag{13}$$

where ($\tilde{\upsilon}^0_{v'\leftarrow v''}$) is the band origin of the vibrational band and $\Delta E_{J',J''}$ is the difference in rotational energies in the ground and excited states, depending on the relevant rotational parameters. Relative line intensities (I_{rel}) of spectra at thermal equilibrium were evaluated from

$$I_{\mathrm{rel}} = Cg_{J''}(\mu_+\mu'_+)^2 s(J,\Delta J)\exp(-E(J'')hc/k_BT), \tag{14}$$

where $g_{J''}$ is the degeneracy of level J''. μ_+ and μ'_+ are the one-photon perpendicular transition moments for transitions via a virtual state in the two-photon excitation,[14] treated here as constants. $s(J,\Delta J)$ are relevant Hönl–London factors, which depend on the quantum numbers J' and J''.[47] $E(J'')$ is the rotational energy in the ground state and C is a constant. Individual rotational lines were displayed as Gaussian-shaped functions of wavenumbers ($I(\tilde{\upsilon})$) and bandwidth [bw (cm^{-1})] as[48]

$$I(\tilde{\upsilon}) = \frac{I_{\mathrm{rel}}}{bw}\exp\left(-\frac{4\ln(2)}{bw^2}(\tilde{\upsilon} - \tilde{\upsilon}^0 - \Delta E_{J',J''})^2\right). \tag{15}$$

Assuming the ionization step, following the resonance excitation, to be independent of excitation wavelength, $I(\tilde{\upsilon})$ as a function of $\tilde{\upsilon}$ can be assumed to represent a (2+n) REMPI spectrum.

Calculated spectroscopic parameters, experimental values, as well as values derived by or from Bettendorff *et al.*[27] for the ground state and the $F\,^1\Delta$ state are listed in Tables II and III. In general, average internuclear distances (r_e,r_v), hence rotational constants (B_e,B_v), are found to be well reproduced by the DFT, MP2, MP4, and CC calculations for the ground state, whereas the vibrational frequency (ω_e) is found to be slightly overestimated with the exception of B3LYP calculations, where they are underestimated. For the $F\,^1\Delta$ state the internuclear distance r_e is found to be overestimated by about 0.01–0.02 Å in most calculations; hence the rotational constants are slightly underestimated (by about 0.5–0.6 cm^{-1} for B_0). The vibrational frequency is consistently found to be slightly overestimated. The discrepancies in the rotational and vibrational parameters are larger for the DFT calculations than for the CC calculations. The electronic excitation energy (T_0) is overestimated in the EOM-CC calculations, whereas it is underestimated in the DFT calculations. The latter effect is explained by too rapid decay of conventional exchange-correlation functionals as opposed to the theoretical $-1/r$ asymptotic decay.[49] However, as already the ground-state geometry and thus rotational constant exhibited a larger deviation from the experimental than the MP/CC results, we opted against improving the TD-DFT excitation energies by asymptotical corrections[50] to the functionals. Generally the CC calculations, compared to the TD-DFT calculations, were found to give parameters closer to that observed, as one might expect. All in all, the use of the largest basis set aug-cc-pV5Z and the completely renormalized equation-of-motion CCSD(T) calculation for the excited state gave spectroscopic parameters and potential curve shape closest to that observed experimentally and slightly better than those calculated before by Bettendorff *et al.*[27]

Ab initio REMPI spectra for the $F\,^1\Delta_2(v'=0) \leftarrow\leftarrow X\,^1\Sigma^+(v'=0)$ process [excited state: CR-EOM-CCSD(T)/aug-cc-pV5Z; ground state: CCSD/aug-cc-pV5Z] are shown in Fig. 6 along with the REMPI spectrum obtained by recording $H^{35}Cl^+$ ion signal on a relative two-photon wavenumber scale. The simulated spectrum is also shown in the same figure. Overall rotational structure shapes, in terms of band head shadings (red/blue) and spectral ranges, are reproduced distinctly, whereas finer details are not always reproduced well. The fine structure of the calculated REMPI spectra, presented on a relative two-photon wavenumber scale, is dependent on the calculated rotational parameters

TABLE II. Spectroscopic parameters and their basis set dependence for the ground state of $H^{35}Cl$, $X\,^1\Sigma^+$ derived from various *ab initio* calculations and experiments.

	r_e (Å)	ω_e (cm^{-1})	$\omega_e x_e$ (cm^{-1})	B_0 (cm^{-1})
Experiments	1.27455[a]	2990.946[a,b]	52.8186[a,b]	10.439 826[c]
B3LYP/aug-cc-pVTZ	1.284	2957	57	10.19
B3LYP/aug-cc-pVQZ	1.282	2955	57	10.21
MPW1PW91/aug-cc-pVQZ	1.278	3007	56	10.27
MP2/aug-cc-pVTZ	1.271	3070	56	10.40
MP2/aug-cc-pVQZ	1.272	3055	55	10.39
MP4/aug-cc-pVTZ	1.275	3025	58	10.33
MP4/aug-cc-pVQZ	1.276	3009	57	10.32
CCSD/AQZ	1.273	3030	57	10.36
CCSD/aug-cc-pVTZ	1.273	3053	53	10.36
CCSD/aug-cc-pVQZ	1.274	3042	51	10.53
CCSD/aug-cc-pV5Z	1.268	3079	61	10.44
CCSD/aug-cc-pCVQZ	1.272	3050	52	10.38
CCSD(T)/aug-cc-pVTZ	1.275	3016	58	10.32
CCSD(T)/aug-cc-pVQZ	1.276	3002	57	10.31
CR-CCSD(T)/aug-cc-pVTZ	1.246	3022	58	10.33
CR-CCSD(T)/aug-cc-pVQZ	1.256	3008	56	10.32

[a]Reference 52.
[b]Reference 13.
[c]$B_0=B_e-\alpha_e(1/2)$ for B_e and α_e in Ref. 52.

and on the temperature, which was found to be about 100 K from simulation analysis, but independent of the vibrational ($\omega_e, \omega_e x_e$) and electronic (T_0) parameters. Hence the discrepancy between the calculated and experimental data is mainly due to the underestimation of the rotational constant in the upper state.

The slight but consistent deviations in the calculated compared to the experimentally determined parameters, the internuclear distances ($r_{\text{calc}} > r_{\text{exp}}$), the rotational constants ($B_{\text{calc}} < B_{\text{exp}}$), the electronic parameters, and the vibrational frequencies ($\omega_{\text{calc}} > \omega_{\text{exp}}$) for the excited singlet Δ state suggest that an extra bond stability factor is not taken into account in the calculation procedure. This could be due to Rydberg-Rydberg state interactions. First, the weak perturbation mentioned above for the $F\,^1\Delta_2(v'=1)$, $J'=8$ state has been attributed to a state mixing to give the $F\,^1\Delta_2$ state a slight $\Omega=1$ character, hence a heterogeneous coupling with the $V\,^1\Sigma^+$ ($\Omega=0$) state.[11,14] Second, spin-orbit coupling is found to mix the $F(^1\Delta_2)$ and the $f(^3\Delta_2)$ states.[12,51]

TABLE III. Spectroscopic parameters and their basis-set dependence for the lowest energy singlet delta state, $F\,^1\Delta_2$, of $H^{35}Cl$, derived from various *ab initio* calculations and experiments.

	T_0 (cm^{-1})	r_e (Å)	ω_e (cm^{-1})	$\omega_e x_e$ (cm^{-1})	B_e (cm^{-1})	B_0 (cm^{-1})	B_1 (cm^{-1})
Experiments	81 555.3875[a]	1.295[b]	2608.3[b]	49.35[b]	10.415/ 10.412[c]	10.3246/ 10.3228[d]	10.143/ 10.1447[d]
Bettendorff *et al.*[e]	79 930[e]	1.314[e]	2715[e]/ 2813[e,f]	69[e,f]	9.96[e] 9.68[e,f]	9.42[e,f]	8.90[e,f]
TD-DFT B3LYP/aug-cc-pVTZ	77 810	1.304	2916	75	10.12	9.83	9.27
TD-DFT B3LYP/aug-cc-pVQZ	76 079	1.303	2881	73	10.14	9.86	9.30
TD-DFT MPW1PW91/aug-cc-pVQZ	78 037	1.300	2906	68	10.18	9.90	9.36
EOM-CCSD/AQZ	81 391	1.317	2681	58	9.92	9.65	9.13
EOM-CCSD/aug-cc-pVTZ	84 924	1.311	2731	58	10.02	9.75	9.24
EOM-CCSD/aug-cc-pVQZ	84 219	1.314	2711	58	9.97	9.71	9.19
EOM-CCSD/aug-cc-pV5Z	84 023	1.308	2736	63	10.06	9.79	9.25
EOM-CCSD/aug-cc-pCVQZ	84 635	1.315	2719	59	10.01	9.74	9.22
CR-EOM-CCSD(T)/aug-cc-pVTZ	84 058	1.309	2758	55	10.05	9.79	9.29
CR-EOM-CCSD(T)/aug-cc-pVQZ	83 141	1.312	2736	56	9.99	9.74	9.24
CR-EOM-CCSD(T)/aug-cc-pV5Z	82 707	1.306	2755	61	10.09	9.81	9.28
CR-EOM-CCSD(T)/aug-cc-pCVQZ	83 109	1.311	2740	57	10.02	9.76	9.25

[a]$T_0=v_0-(\omega_e/2-\omega_e x_e/4)$; v_0 from Ref. 6; ω_e, $\omega_e x_e$ from Ref. 14.
[b]Reference 14.
[c]Derived from fitting B_v vs v according to $B_v=B_e-\alpha_e(v+1/2)$ for B_v from Ref. 6.
[d]Reference 6.
[e]Reference 27.
[f]Derived from Morse potential fitting of a published potential curve in Ref. 27.

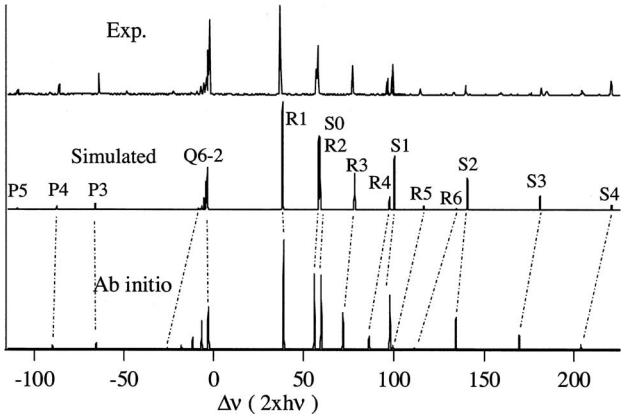

FIG. 6. $(2+n)$ REMPI spectra for HCl corresponding to the two-photon excitation region of 82 730–83 070 cm^{-1} on a relative two-photon wavenumber scale; experimental REMPI spectrum for $H^{35}Cl^+$ (top); simulated two-photon absorption spectrum for the $F\,^1\Delta_2(v'=0) \leftarrow\leftarrow X\,^1\Sigma^+(v'=0)$ transition, using rotational constants derived from experimental data (Ref. 14) and rotational temperature, $T_{rot}=100$ K (middle); *ab initio* REMPI spectrum for the $F\,^1\Delta_2(v'=0) \leftarrow\leftarrow X\,^1\Sigma^+(v'=0)$ transition derived from the use of potential curves calculated for the basis set aug-cc-pV5Z and the CR-CCSD(T) calculation for the excited state (bottom). Numbers for rotational lines refer to J'' quantum numbers.

CONCLUSIONS

Ion-mass spectra were recorded as a function of two-photon wavenumbers corresponding to $(2+n)$ REMPI to obtain 2D REMPI data for HCl (for natural abundance isotopomers $H^{35}Cl:H^{37}Cl \sim 75:25$). Mass-resolved REMPI spectra were obtained for the ion species H^+, $^{35}Cl^+$, $H^{35}Cl^+$, $^{37}Cl^+$, and $H^{37}Cl^+$ in the two-photon wavenumber region of 82 600–88 100 cm^{-1}. Contour representations of the data are found to be very useful for assigning the fine structure of rotationally resolved REMPI spectra for both isotopomers. Emphasis was placed on analysis of data relevant to ionizations via resonance excitation to the $F(^1\Delta_2)(v'=0,1,2)$ Rydberg states and the $V\,^1\Sigma^+$ ion-pair states close in energy, in order to explore the mechanisms of photorupture (photodissociation and photoionization) channels. H^iCl^+; $i=35,37$ and H^+ but no $^iCl^+$; $i=35,37$ ions were observed for excitations via all the rovibrational states $F(^1\Delta_2)(v'=0,1,2)$ except for $F(^1\Delta_2)(v'=1)$, $J'=8$, with H^iCl^+ ions as the dominating product. For $F(^1\Delta_2)(v'=1)$, $J'=8$ significant amount of all ions were detected. This effect, along with anomalies observed in relative ion intensities for excitations via the $V\,^1\Sigma^+(v'=14)$, $J'=8$, as well as observed rotational line shifts, is in agreement with a near-resonance state interaction, $F(^1\Delta_2)(v'=1)$, $J'=8 \leftrightarrow V\,^1\Sigma^+(v'=14), J'=8$, and gives an important indication of how photoionization channels depend on the resonance intermediate states. Power dependence measurements for ion signals further support the proposed photorupture mechanism as presented schematically in Figs. 1(a) and 1(b) and described above.

Cl^+ ion formation is characteristic for ion-pair state involvements in the ionization processes of HCl. HCl^+ ion formation is largely indicative of the Rydberg state involvement. This rather clear distinction between the two ionization channels in terms of measurable signals allowed estimates of the state fractions in the $F(^1\Delta_2)(v'=1)$, $J'=8 \leftrightarrow V\,^1\Sigma^+(v'=14)$, $J'=8$ mixing for $H^{35}Cl$ and $H^{37}Cl$. The fraction evaluations coupled with a perturbation treatment for a level-to-level interaction further allowed state interaction strengths to be evaluated. We performed *ab initio* calculations at several levels with a number of basis sets to derive potential energy curves for the ground and excited singlet states. Morse fit analysis of the ground state and the lowest energy $^1\Delta$ state was used to evaluate the vibrational and rotational spectroscopic parameters, as well as to calculate two-photon absorption spectra. Calculated parameters and spectra were compared with experimentally evaluated parameters and REMPI spectra as well as with older *ab initio* calculations. Slight but significant variations in parameters and finer detailed spectroscopic structures are attributed partly to lack of state interaction assumptions in the calculations.

ACKNOWLEDGMENTS

The financial support of the University Research Fund, University of Iceland and the Icelandic Science Foundation, is gratefully acknowledged.

[1] S. G. Tilford, M. L. Ginter, and J. T. Vanderslice, J. Mol. Spectrosc. **33**, 505 (1970).
[2] S. G. Tilford and M. L. Ginter, J. Mol. Spectrosc. **40**, 568 (1971).
[3] D. S. Ginter and M. L. Ginter, J. Mol. Spectrosc. **90**, 177 (1981).
[4] J. B. Nee, M. Suto, and L. C. Lee, J. Chem. Phys. **85**, 719 (1986).
[5] T. A. Spiglanin, D. W. Chandler, and D. H. Parker, Chem. Phys. Lett. **137**, 414 (1987); H. Wang and Á. Kvaran, J. Mol. Struct. **563–564**, 235 (2001).
[6] D. S. Green, G. A. Bickel, and S. C. Wallace, J. Mol. Spectrosc. **150**, 303 (1991).
[7] D. S. Green, G. A. Bickel, and S. C. Wallace, J. Mol. Spectrosc. **150**, 354 (1991); Á. Kvaran, H. Wang, and Á. Logadóttir, in Recent Res. Devel. in Physical Chem., **2**, 233 (1998).
[8] D. S. Green, G. A. Bickel, and S. C. Wallace, J. Mol. Spectrosc. **150**, 388 (1991).
[9] D. S. Green and S. C. Wallace, J. Chem. Phys. **96**, 5857 (1992).
[10] E. de Beer, B. G. Koenders, M. P. Koopmans, and C. A. de Lange, J. Chem. Soc., Faraday Trans. **86**, 2035 (1990).
[11] Y. Xie, P. T. A. Reilly, S. Chilukuri, and R. J. Gordon, J. Chem. Phys. **95**, 854 (1991).
[12] E. de Beer, W. J. Buma, and C. A. de Lange, J. Chem. Phys. **99**, 3252 (1993).
[13] Á. Kvaran, Á. Logadóttir, and H. Wang, J. Chem. Phys. **109**, 5856 (1998).
[14] Á. Kvaran, H. Wang, and Á. Logadóttir, J. Chem. Phys. **112**, 10811 (2000).
[15] Á. Kvaran, H. Wang, and B. G. Waage, Can. J. Phys. **79**, 197 (2001).
[16] Á. Kvaran and H. Wang, Mol. Phys. **100**, 3513 (2002).
[17] Á. Kvaran and H. Wang, J. Mol. Spectrosc. **228**, 143 (2004).
[18] A. J. Yencha, D. Kaur, R. J. Donovan, Á. Kvaran, A. Hopkirk, H. Lefebvre-Brion, and F. Keller, J. Chem. Phys. **99**, 4986 (1993).
[19] C. Romanescu, S. Manzhos, D. Boldovsky, J. Clarke, and H. P. Loock, J. Chem. Phys. **120**, 767 (2004).
[20] A. I. Chichinin, C. Maul, and K. H. Gericke, J. Chem. Phys. **124**, 224324 (2006).
[21] A. I. Chichinin, P. S. Shternin, N. Godecke, S. Kauczok, C. Maul, O. S. Vasyutinskii, and K. H. Gericke, J. Chem. Phys. **125**, 034310 (2006).
[22] C. Romanescu and H. P. Loock, J. Chem. Phys. **127**, 124304 (2007).
[23] A. J. Yencha, A. J. Cormack, R. J. Donovan, A. Hopkirk, and G. C. King, Chem. Phys. **238**, 109 (1998).
[24] B. Retail, R. A. Rose, J. K. Pearce, S. J. Greaves, and A. J. Orr-Ewing, Phys. Chem. Chem. Phys. **10**, 1675 (2008); S. J. Dixon-Warren, R. C. Jackson, J. C. Polanyi, H. Rieley, J. G. Shapter, and H. Weiss, J. Phys. Chem. **96**, 10983 (1992); R. C. Jackson, J. C. Polanyi, and P. Sjövall, J. Chem. Phys. **102**, 6308 (1995); J. K. Pearce, B. Retail, S. J. Greaves, R. A. Rose, and A. J. Orr-Ewing, J. Phys. Chem. A **111**, 13296 (2007); M. J. Bass, M. Brouard, C. Vallance, T. N. Kitsopoulos, P. C. Samartzis, and

R. L. Toomes, J. Chem. Phys. **121**, 7175 (2004); M. J. Bass, M. Brouard, C. Vallance, T. N. Kitsopoulos, P. C. Samartzis, and R. L. Toomes, *ibid.* **119**, 7168 (2003).
[25] W. C. Price, Proc. R. Soc. London, Ser. A **167**, 216 (1938).
[26] R. Liyanage, R. J. Gordon, and R. W. Field, J. Chem. Phys. **109**, 8374 (1998).
[27] M. Bettendorff, S. D. Peyerimhoff, and R. J. Buenker, Chem. Phys. **66**, 261 (1982).
[28] D. M. Hirst and M. F. Guest, Mol. Phys. **41**, 1483 (1980).
[29] A. D. Pradhan, K. P. Kirby, and A. Dalgarno, J. Chem. Phys. **95**, 9009 (1991); **103**, 864 (1995).
[30] T. H. Dunning, J. Phys. Chem. A **104**, 9062 (2000); C. E. Smith, R. A. King, and T. D. Crawford, J. Chem. Phys. **122**, 054110 (2005); R. J. Bartlett and M. Musial, Rev. Mod. Phys. **79**, 291 (2007).
[31] S. R. Gwaltney, M. Nooijen, and R. J. Bartlett, Chem. Phys. Lett. **248**, 189 (1996).
[32] J. Pitarch-Ruiz, A. S. de Meras, J. Sanchez-Marin, A. M. Velasco, C. Lavin, and I. Martin, J. Phys. Chem. A **112**, 3275 (2008).
[33] M. G. White, G. E. Leroi, M.-H. Ho, and E. D. Poliakoff, J. Chem. Phys. **87**, 6553 (1987); H. Frohlich and M. Glassmaujean, Phys. Rev. A **42**, 1396 (1990).
[34] H. Lefebvre-Brion and F. Keller, J. Chem. Phys. **90**, 7176 (1989).
[35] Á. Kvaran, K. Matthíasson, and H. Wang, Physical Chemistry; An Indian Journal **1**(1), 11 (2006); Á. Kvaran, Ó. F. Sigurbjörnsson, and H. Wang, J. Mol. Struct. **790**, 27 (2006).
[36] R. J. Donovan, R. V. Flood, K. P. Lawley, A. J. Yencha, and T. Ridley, Chem. Phys. **164**, 439 (1992).
[37] G. Herzberg, *Molecular Spectra and Molecular Structure: I. Spectra of Diatomic Molecules*, 2nd ed. (Van Nostrand Reinhold, New York, 1950).
[38] H. Lefebvre-Brion and R. W. Field, *Perturbations in the Spectra of Diatomic Molecules* (Academic, London, 1986).
[39] M. J. Frisch, G. W. Trucks, H. B. Schlegel *et al.*, GAUSSIAN 03 (Gaussian, Inc., 2004).
[40] E J. Bylaska, W A. deJong, N. Govind, K. Kowalski, T. P. Straatsma, M Valiev, D. Wang, E. Apra, T. L. Windus, J. Hammond, P. Nichols, S. Hirata, M. T. Hackler, Y. Zhao, P.-D. Fan, R. J. Harrison, M. Dupuis, D M. A. Smith, J. Nieplocha, V. Tipparaju, M. Krishnan, Q. Wu, T. Van-Voorhis, A. A. Auer, M. Nooijen, E. Brown, G. Cisneros, G. I. Fann, H. Fruchtl, J. Garza, K. Hirao, R. Kendall, J. A. Nichols, K. Tsemekhman, K. Wolinski, J. Anchell, D. Bernholdt, P. Borowski, T. Clark, D. Clerc, H. Dachsel, M. Deegan, K. Dyall, D. Elwood, E. Glendening, M. Gutowski, A. Hess, J. Jaffe, B. Johnson, J. Ju, R. Kobayashi, R. Kutteh, Z. Lin, R. Littlefield, X. Long, B. Meng, T. Nakajima, S. Niu, L. Pollack, M. Rosing, G. Sandrone, M. Stave, H. Taylor, G. Thomas, J. vanLenthe, A. Wong, and Z. Zhang, NWCHEM, A Computational Chemistry Package for Parallel Computers, Version 5.1 (Pacific Northwest, National Laboratory, Richland, Washington 99352-0999, USA, 2007); E. J. Bylaska, W. A. deJong, K. Kowalski, T. P. Straatsma, M. Valiev, D. Wang, E. Apra, T. L. Windus, S. Hirata, M. T. Hackler, Y. Zhao, P.-D. Fan, R. J. Harrison, M. Dupuis, D. M. A. Smith, J. Nieplocha, V. Tipparaju, M. Krishnan, A. A. Auer, M. Nooijen, E. Brown, G. Cisneros, G. I. Fann, H. Fruchtl, J. Garza, K. Hirao, R. Kendall, J. A. Nichols, K. Tsemekhman, K. Wolinski, J. Anchell, D. Bernholdt, P. Borowski, T. Clark, D. Clerc, H. Dachsel, M. Deegan, K. Dyall, D. Elwood, E. Glendening, M. Gutowski, A. Hess, J. Jaffe, B. Johnson, J. Ju, R. Kobayashi, R. Kutteh, Z. Lin, R. Littlefield, X. Long, B. Meng, T. Nakajima, S. Niu, L. Pollack, M. Rosing, G. Sandrone, M. Stave, H. Taylor, G. Thomas, J. van Lenthe, A. Wang, and Z. Zhang, NWCHEM, A Computational Chemistry Package for Parallel Computers, Version 5.0 (Pacific Northwest National Laboratory, Richland, Washington 99352-0999, USA., 2006); R. A. Kendall, E. Apré, D. E. Bernholdt, E. J. Bylaska, M. Dupuis, G. I. Fann, R. J. Harrison, J. Ju, J. A. Nichols, J. Nieplocha, T. P. Straatsma, T. L. Windus, and A. T. Wang, Comput. Phys. Commun. **128**, 260 (2000).
[41] J. F. Stanton, J. Gauss, J. D. Watts, W. J. Lauderdale, and R. J. Bartlett, Int. J. Quantum Chem., Quantum Chem. Symp. **26**, 879 (1992).
[42] J. F. Stanton and R. J. Bartlett, J. Chem. Phys. **98**, 7029 (1993).
[43] K. Kowalski and P. Piecuch, J. Chem. Phys. **120**, 1715 (2004).
[44] T. H. Dunning, Jr., J. Chem. Phys. **90**, 1007 (1989); R. A. Kendall, T. H. Dunning, Jr., and R. J. Harrison, *ibid.* **96**, 6796 (1992); D. E. Woon and T. H. Dunning, Jr., *ibid.* **98**, 1358 (1993).
[45] K. A. Peterson and T. H. Dunning, Jr., J. Chem. Phys. **117**, 10548 (2002).
[46] D. Feller, J. Comput. Chem. **17**, 1571 (1996); K. L. Schuchardt, B. T. Didier, T. Elsethagen, L. Sun, V. Gurumoorthi, J. Chase, J. Li, and T. L. Windus, J. Chem. Inf. Model. **47**, 1571 (2007).
[47] R. G. Bray and R. M. Hochstrasser, Mol. Phys. **31**, 1199 (1976).
[48] Á. Kvaran, H. Wang, and J. Ásgeirsson, J. Mol. Spectrosc. **163**, 541 (1994).
[49] M. E. Casida, C. Jamorski, K. C. Casida, and D. R. Salahub, J. Chem. Phys. **108**, 4439 (1998).
[50] S. Hirata, C. G. Zhan, E. Apra, T. L. Windus, and D. A. Dixon, J. Phys. Chem. A **107**, 10154 (2003); C. G. Zhan, J. A. Nichols, and D. A. Dixon, *ibid.* **107**, 4184 (2003).
[51] Y.-F. Zhu, E. R. Grant, K. Wang, V. McKoy, and H. Lefebvre-Brion, J. Chem. Phys. **100**, 8633 (1994).
[52] K. P. Huber and G. Herzberg, *Constants of Diatomic Molecules* (Van Nostrand-Reinhold, New York, 1979).